

FLAT: An Optimized Dataflow for Mitigating Attention Bottlenecks

Sheng-Chun Kao¹, Suvinay Subramanian², Gaurav Agrawal², Amir Yazdanbakhsh² and Tushar Krishna¹

¹Georgia Institute of Technology

²Google

¹*skao6@gatech.edu, tushar@ece.gatech.edu*

²*{suvinay, chippguy, ayazdan}@google.com*

Abstract

Attention mechanisms, primarily designed to capture pairwise correlations between words, have become the backbone of machine learning, expanding beyond natural language processing into other domains. This growth in adaptation comes at the cost of prohibitively large memory requirements and computational complexity, especially at higher number of input elements. This limitation is due to inherently limited data reuse opportunities and quadratic growth in memory footprints, leading to severe memory-boundedness and limited scalability of input elements. This work addresses these challenges by devising a tailored dataflow optimization, called FLAT, for attention mechanisms without altering their functionality. This dataflow processes costly attention operations through a unique fusion mechanism, transforming the memory footprint quadratic growth to merely a linear one. To realize the full potential of this bespoke mechanism, we propose a tiling approach to enhance the data reuse across attention operations. Our method both mitigates the off-chip bandwidth bottleneck as well as reduces the on-chip memory requirement. Across a diverse range of models, FLAT delivers $1.94\times$ ($1.76\times$) speedup and 49% and (42%) of energy savings compared to the state-of-the-art edge (cloud) accelerators with no customized dataflow optimization. Our evaluations demonstrate that state-of-the-art DNN dataflows applied to attention operations reach the efficiency limit for inputs above 512 elements. In contrast, FLAT unblocks transformer models for inputs with up to 64 K elements in edge and cloud accelerators.

1. Introduction

Attention mechanisms, the key building block of transformer models, have enabled state-of-the-art results across a wide range of machine learning (ML) tasks—from natural language processing (NLP) [22, 53, 81], to object detection [12, 75, 102], image classification [30, 93, 99, 101], image generation [13, 26, 60], and music synthesis [36, 37]. This exponential growth of transformer models are expected to serve as the foundation of a new breed of machine learning models in the upcoming years. A key attribute of attention-based models is the *sequence length* (N) defining the number of input elements for which

a pairwise correlation scores is computed. Intuitively, increasing sequence length enables the attention-based models to better capture the context of input sentences or the relation between image segments. The demand for leveraging long-sequence (e.g. $N = 8K$ to $N = 69K$) attention-based models has already emerged in ML community [79], beyond natural language understanding [64] into protein folding [20] and text summarization [48] and audio generation [55].

Compared to existing convolutional [15, 16, 25, 71] and fully-connected neural network accelerators [62], architecting accelerators for attention-based models poses different design challenges, mainly attributed to their soaring demand for on-chip memory and compute complexities. Recent proposed accelerators for attention-based models [32, 33] have mainly relied on algorithmic optimizations, often with negative repercussion on model accuracy. Algorithmic techniques in practice include sparsification or compressing the attention blocks [11, 18, 19, 20, 21, 22, 45, 48, 61, 63, 64, 67, 73, 78, 87] and/or leveraging lossy approximation computation [32, 33, 85].

In this work, we identify that the conventional dataflow/mapping methods for CONV and FC layers [1, 15, 25, 43] are inadequate for attention layers. This is because the main operators within attention layers exhibit distinct compute and memory characteristics posing notable bottlenecks on off-chip memory bandwidth compared to CONV and FC. We identify the following challenges in devising dataflow optimizations for attention layers:

- (1) **Significantly low operational intensity.** Inherently low data reuse in activation-activation operators significantly reduces the operational density of such operators in attention layers. This inherently low operational density subsequently makes the activation-activation operators *fundamentally* memory-bound. While prior work on intra-operator dataflow optimization, such as loop transformation and scheduling techniques [1, 16, 25, 50, 51, 59], targets CONV and batched FC operators by leveraging the ample intrinsic data reuse, which are not well-suited for activation-activation operators lacking data reuse opportunity.
- (2) **Complex many-to-many operators.** The main at-

tention operators have many-to-many relation, obscuring opportunities to use operator fusion [58] in attention operators. That is because operator fusion in conventional ML compilers [6, 14, 66] mainly target operations such as CONV and FC with one-to-one (i.e. element-wise) relation.

- (3) **Prohibitively large intermediate tensors.** The size of intermediate tensors in attention layers grows quadratically— $\mathcal{O}(N^2)$ [19, 20, 22, 45, 53, 81, 87]—with the sequence length. This quadratic growth imposes a significant pressure on on-chip memory capacity and prohibits opportunities to store the intermediate results on-chip and improve the compute utilization, a common practice in CNN accelerators [15].

This paper fundamentally tackles the challenges associated with attention layers by devising a first in its class *many-to-many inter-operator* dataflow optimization mechanism, called **Fused Logit Attention Tiling**. This optimization particularly fuses multiple many-to-many tensor operator, while systematically preserving their inter-operator data dependencies, leading to a significant reduction on off-chip memory bandwidth pressure. In addition, to fully realizing the performance benefit of this inter-operator fusing mechanism, FLAT performs a new tiling approach across the fused operators. This tiling enables efficient staging of quadratically growing intermediate tensors of attention operations on tight-budgeted on-chip memories, leading to higher performance and energy savings and elevates the scalability of transformer models up to 64 K inputs. These benefits are unlocked with only modest hardware changes, integrating into a platform deployable on off-the-shelf DNN accelerators. In summary, this paper presents the following specific contributions for attention-based models:

- We systematically study the operational intensity of different operators within attention layers and characterize the fundamental roadblocks imposed by limited hardware resources to improve the overall realized performance of attention accelerators (§3).
- Based on the resulting findings, we explore fusion opportunities between different operators in attention layers and justify our proposed many-to-many inter-operator fusion (§4). While beneficial, this fusion inflicts a fundamental challenge of preserving the inter-operator data dependencies, imposed by the softmax operation. To address, we expound our tailored dataflow optimization approach for attention layers, enabling higher data reuse of the quadratically growing intermediate attention tensors from low-capacity but high-bandwidth on-chip memory. We show that this dataflow optimization efficiently mitigates the pressure on off-chip memory bandwidth, leading to a higher performance and energy efficiency in accelerators (§5).
- We develop a map-space exploration framework to ef-

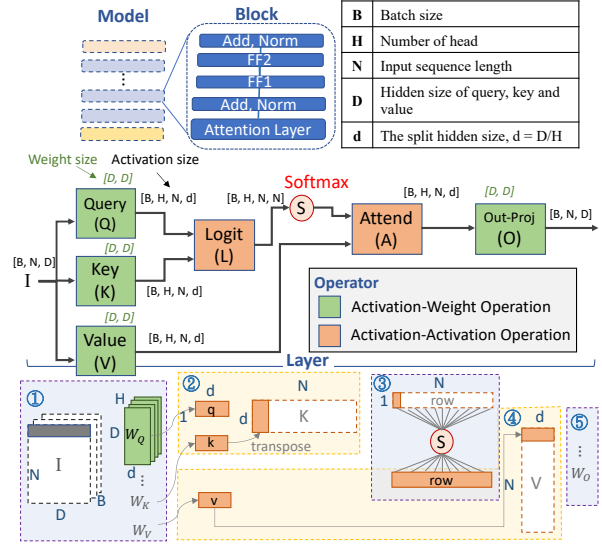


Fig. 1: The structure of attention-based models. Green matrix notation shows the size of weight tensors; black matrix notation shows the size of activation tensors; Softmax is applied on output of Logit.

ficiently search for optimal loop orders across fused operators and tiling sizes. This framework optimizes performance metrics of interest subject to different hardware resource constraints, such as number of processing elements and on-chip memory capacity (§6).

We evaluate FLAT on a variety of Attention-based models, including BERT [82], TrXL [53], FlauBERT [54], T5 [65], and XLNet [53], for both an edge and cloud accelerators. Compared to a range of state-of-the-art dataflow optimizers, FLAT delivers $1.75\times$ and $1.65\times$ speedup and 44% and 55% energy savings for recent edge and cloud accelerators, respectively. Furthermore, our results show that while the conventional DNN dataflow optimizers for attention operations bumps up against the efficiency limit for inputs above 512 elements, our dataflow optimization tailored for attention operations unblocks the scalability of transformer models for significantly larger input sizes, up to 64 K elements.

2. Background

2.1. Attention-based Models

Terminology. Transformer models [54, 76, 82] generally share similar architectures. In a top-down view (Figure 1), an attention-based **model** comprises multiple (often identically parameterized) attention **blocks**¹. An attention block comprises multiple **layers**: an attention layer, a normalization layer, followed by multiple (typically two) fully connected layers. Finally, each layer comprises one

¹Models may include other blocks: an embedding block with positional encoding and masking, and a few task-specific FC or CONV layers.

or more **operations** or **operators**.

Computation operators. The attention mechanism measures how closely two *tokens* are related in an input *sequence*. Each token in the input sequence is represented as a vector of dimension D , each sequence has N tokens, and an input batch to an attention layer comprises a batch of B sequences; thus the input to the attention layer is a tensor of dimension $[B, N, D]$. **Figure 1** (bottom) highlights the flow of a single token vector (of dimension D) through the attention mechanism. Step ①, three vectors are derived for each token’s vector in the input: called Key (K), Query (Q), Value (V). This is achieved by multiplying the input tensor with learnable weight matrices. Attention mechanisms often use multiple *heads* to generate H such K, Q, V vectors for each token vector in the input. Thus each of K, Q, V generates a tensor of dimension $[B, H, N, d]$. Step ②, we compute the *logits score* (L) which captures how strongly each token is related to each other token in the sequence. This is done by a (d -dim) dot product of each vector of the key with the corresponding vector of the query. Each dot product yields a single scalar score, but this score is computed for each token against all other tokens in the sequence yielding an output tensor of dimension $[B, H, N, N]$. Step ③, the logits scores then needs to be normalized. While there are several normalization functions, they all share key traits. The normalization is done across a *row* of N logits scores in each sequence: to generate a row of N normalized scores, the normalization operator reads N input scores, performs a reduction of these N scores, and scales each of the N input scores by the reduced value. We use softmax since it is the most commonly used normalization function. Step ④, involves performing a weighted sum of the value vectors with the corresponding weights from the logits, which yields an output tensor $[B, H, N, d]$. Finally, step ⑤ concatenates the attention outputs from the H heads and with its weight matrix computes a output tensor $[B, N, D]$. These complete an attention layer.

This can be represented succinctly as the computational graph in **Figure 1**, comprising the following operators: i) Query (Q), Key (K), and Value (V) operators that perform a projection of the input tensor, ii) Logit (L) and Attend (A) operators that compute the logits scores and weighted-sum of values respectively, and iii) Output (O) operator that performs an output projection. We categorize them into two: (i) activation-weight operators (Q, K, V, O), which operate on activation tensors (from previous operators) and weight tensors (model parameters) and perform a GEMM computation as conventional fully connected operators (FCs), and ii) activation-activation operators (L, A), which operate on two activations from different previous operators and perform a GEMM computation. The L and A operators often dominate the latency and power consumption while running the model [32], and

even more so at long sequence lengths, as shown in our evaluations (**Figure 15**).

2.2. DNN Accelerators - Performance Considerations

We consider spatial DNN accelerators [15, 50] in this work (§7.3 provides more details). We discuss the key factors that determine the realized performance when running a DNN model on an accelerator with specific hardware resources (PEs, on-chip memory size and off-chip memory BW).

2.2.1. Operational Intensity | Roofline Performance

Operational intensity is an indicator of the maximum possible performance of an *individual* operator given a set of hardware resources. The operational intensity of an operator is defined as the number of arithmetic operations divided by the number of memory accesses. A lower operational intensity implies an operator has fewer opportunities for data reuse and is more likely to be memory bandwidth(BW)-bounded. This directly decides the roofline (or best achievable) performance of the operator on the underlying accelerator.

$$Op. Int. = \frac{num. of operations}{num. of memory accesses} \quad (1)$$

2.2.2. Dataflow | Realized Performance

Dataflow refers to the mechanisms to stage data from the off-chip memory through the on-chip memory hierarchy to the compute PEs, over space and time [50]. It determines the actual achieved performance. Since memory access is often the bottleneck in executing DNN operators [77], the dataflow exposes data reuse opportunities across operands that can be exploited in hardware via buffering and data forwarding/broadcast [50]. Formally, the *dataflow* encompasses: (i) tiling (how tensors are sliced, stored and fetched across the memory hierarchy), (ii) compute order (order in which loop iterations are performed), and (iii) parallelism (how compute is mapped across PEs spatially). The dataflow along with specific tile sizes is often called a *mapping* [50, 51].

3. Challenges with Running Attention Layers

3.1. Challenge 1: Low Operational Intensity of L/A

We start by studying the computational attributes of *individual* operators within attention layers.

3.1.1. Activation-Weight Operators (Q/K/V/O) For Q/K/V/O operators, following the notation in **Figure 1**, the number of operations is $O(BND^2)$. The number of memory accesses for the input (activations), weight (parameters), and output (activations) tensors are $O(BND)$, $O(D^2)$, $O(BND)$, respectively. Therefore the operational intensity is $O(\frac{BND^2}{BND+D^2+BND})$. We see that increasing the batch size (B) can increase the operational intensity—the

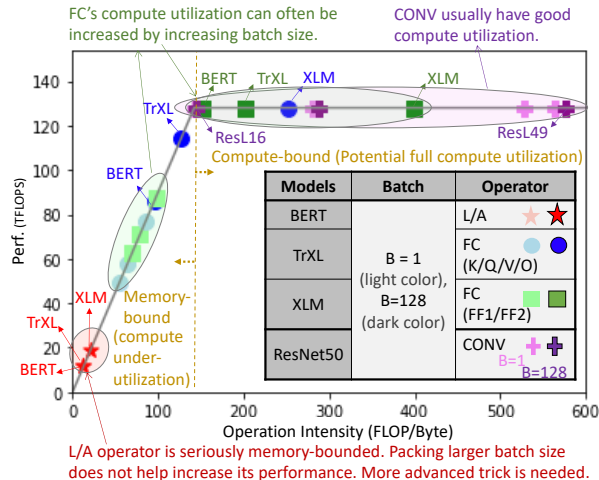


Fig. 2: Roofline analysis on TPU-v3 [42] for operators in BERT(-base) [81], TrXL(-large) [22], and XLM(xlm-mem) [53], and ResNet50 [34] using sequence length = 512.

same weight value can be *reused* by multiple activations, leading to lower BW pressure. This is a typical technique used in activation-weight operators (e.g., CONV and FC, the staple in most DNN models) as it makes better use of the scarce memory bandwidth in accelerators and enables higher utilization of the provisioned compute FLOPs, leading to improved throughput. The specific mechanism to exploit the operational intensity is called dataflow [15, 50].

3.1.2. Activation-Activation Operators (L/A) For L and A operators, the number of operations is $O(BN^2D)$. The number of memory access for the two input-activations and the output-activations are $O(BND)$, $O(BND)$, $O(BN^2)$, respectively. Therefore the operational intensity is $O(\frac{BN^2D}{2BND+BN^2})$. Embedding size (D) is decided by the model, and sequence length (N) is decided by the application. Furthermore, multi-head attention is an often-used variant of the attention mechanism: it leads to higher accuracy in many tasks [81]. It splits the output of the Q/K/V operator along a hidden dimension, reshaping it from size [N, D] to [H, N, d], where $d=D/H$. The operational intensity of L, A becomes $O(\frac{BN^2D}{2BND+BHN^2})$. For these operators, one can not simply increase the batch size to increase the operational intensity.

3.1.3. Roofline Analysis To quantitatively demonstrate the effect of operation intensity across different operators, we show the roofline analysis of operators of three common attention-based models [22, 53, 81] and a widely used CNN network ResNet50 [34] on TPU-v3 [42] in Figure 2. We can see that CONV operators lie in the compute-bound region. FC operators scatter across both memory and compute bound region; however, with the increase in batch size, their operation intensity increases and become compute-bound. This demonstrates why batching is a

(a) Operator Type	Example	Diagram
One-to-One Operator	Element-wise Operator (E.O., e.g., <i>Relu</i> , <i>Add</i>)	
Many-to-Many Operator	Tensor-wise Operator (T.O., e.g., <i>CONV</i> , <i>FC</i> , <i>Softmax</i> , <i>MaxPool</i>)	

● : Operators, : Activations

XLA, Halide, TVM, NVIDIA FasterTransformer[4][5], ...

(b)	Element-wise Operator	Tensor-wise Operator
Element-wise Operator	Element-Element Fusion	Element-Tensor Fusion
Tensor-wise Operator	Tensor-Element Fusion	(c) Tensor-Tensor Fusion

(c) T-T Fusion	Fused-CNN[8], TGPA[94]	This work
Tensor Operator Property	Activation-Weight High Opt. Int. (CONV, FC)	Activation-Activation Low Opt. Int. (L, A)
Intermediate Operator Type	One-to-One (Relu)	Many-to-Many (Softmax)
Domain (Example)	CNNs (CONV-Relu-CONV)	Transformers (L-softmax-A)

Fig. 3: (a) Type of Operator, (b) Type of Operator-Fusion, and (c) Type of Tensor-Tensor Fusion.

popular technique for FC layers. In contrast, L and A operators sit at memory-bound and low-performance region, and batch size increase is not effective in these operators (§3.1.2).

In summary, low operational intensity of the individual L/A operators makes them fundamentally memory-bound, and any dataflow/mapping exploration at the individual operator level cannot further improve performance.

3.2. Challenge 2: Complexity of Op Fusion for L/A

Given the low operational intensity for L/A operators, fusion is an attractive technique to stage the intermediate tensor data on-chip and leverage the higher on-chip memory bandwidth. Operator fusion is an optimization that schedules back-to-back operators together such that the producer’s output directly feeds the consumer, thus avoiding materialization of full intermediate tensor in memory. By avoiding off-chip data movement of the intermediate tensor, we can use the higher on-chip bandwidth to enable improved performance for the fused operator (as opposed to executing the operators individually).

When exploring operation fusion opportunities, we can either fuse among Element-wise Operators (E.O.) or Tensor-wise Operators (T.O.), as shown in Figure 3.

	The Intermediate Tensor Size between L and A Operator		
	BERT	TrXL	XLM
Seq len:512	10 (MB)	10 (MB)	12 (MB)
Seq len:2K	136 (MB)	136 (MB)	144 (MB)
Seq len:16K	8.2 (GB)	8.2 (GB)	8.3 (GB)

Fig. 4: Intermediate tensor size between L and A operators in BERT(-base) [81], TrXL(-large) [22], and XLM(xlm-mem-en) [53].

Element-Element fusion (E-E) is the simplest fusion optimization. With increased interest in operation fusion, more ML compilers/frameworks today support Tensor-Element (T-E) or Element-Tensor (E-T) fusion [6, 10, 14, 49, 66] where *MatMul operators* (i.e., CONV or FC) are often fused with element-wise operators (such as ReLu or Add), reshapes, or shuffling operators [58]

However, Tensor-Tensor Fusion (T-T) is not done automatically. The key reason is that T.O. is a many-to-many operator (Figure 3(a)). While it is often straightforward and a simple engineering exercise to fuse a T.O. with one-to-one operator like E.O., how to fuse many-to-many with other many-to-many and whether it is beneficial to fuse them is still a research question [58]. Indeed, DNN-fusion [58] which studied T-T as recently as PLDI 2021, reported it to be either too complicated or unprofitable. The key reason is that the additional complexity to maintain dependence and stage data (grey intermediate data as shown in Figure 3(b)) could end up negatively impacting register and cache usage [58].

Some previous research papers [8, 91] have discussed Tensor-Fusion in CNNs with the fusion pattern T-(one-to-one)-T such as CONV-Relu-CONV and shown huge potential gain with a well-designed inter-operator dataflow for Tensor-Fusion. This is highlighted in Figure 3(c). However, Tensor-Fusion for attention-based models has not been explored to date, to the best of our knowledge. The complexity of its fusion pattern, T-(many-to-many)-T, makes it much more challenging than for CNNs. *To address this challenge, we design a specialized inter-operator dataflow that not only considers the data dependency of two large tensor operators but also tackles the additional complex data dependency incurred by the many-to-many intermediate activation (§5.2).*

3.3. Challenge 3: Tensor Footprint of L/A

There is one other challenge that is unique to L/A when considering Tensor-Fusion —namely a *quadratic* intermediate tensor footprint. From Figure 1 we can calculate the intermediate tensor between L and A operators has size $O(BHN^2)$ (M-Gran in Table 1). This footprint grows quadratically with sequence length, and exceeds 8GB (exceeding the viable on-chip memory in many data-center class accelerators [42, 80]) beyond sequence lengths of 16K (Figure 4). As NLP tasks with larger sequence lengths become popular [20, 48, 64], the technique of keep-

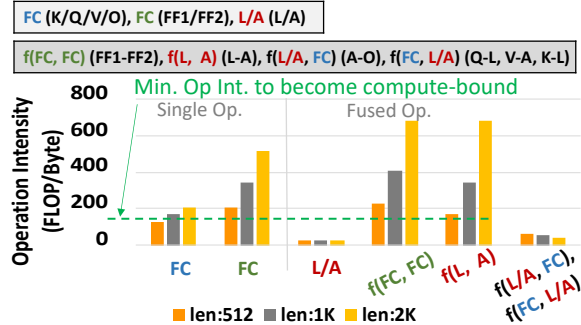


Fig. 5: Potential of Tensor-Tensor Fusion. The operation intensity of single and fused operators in attention layers in TrXL(-large) [22] using batch size=1. The notations are from Figure 1. $f(X, Y)$ means a fused X and Y operator.

ing the entire intermediate tensor on-chip is not scalable. *To address this, we propose a tiling technique for our fused operator that allows controlling the active memory footprint based on the on-chip memory constraint.*

4. FLAT Dataflow Concept

We design a specialized dataflow strategy, Fused Logit Attention Tiling (FLAT), targeting the two memory BW-bound operators in the attention layer, L and A. FLAT includes both intra-operator dataflow and a specialized inter-operator dataflow, executing L and A in concert.

4.1. Identifying Tensor Fusion Opportunity

Figure 5 plots the operation intensity of single and fused operators in attention layers of an attention-based model [22]. The green dotted line marks the operation intensity threshold (ridge point) from memory to compute boundedness in TPU-v3 [42]. We observe that for FC-based operators (K/Q/V/O), the operational intensity is sufficient to be compute-bound, while for L/A it is low (as we had also observed via Figure 2). However, after fusing L and A ($f(L, A)$), the effective operational intensity (of the fused operator) is higher. This motivates us to explore L and A fusion.

Why not fuse other operators? We did not fuse other operator pairs such as $f(Q, L)$, $f(A, O)$, or $f(V, A)$, for three reasons. (1) The operational intensity is often sufficient and can be increased by leveraging batch size to reach compute-bound (Figure 2). (2) Fusing two FCs ($f(FC, FC)$) can achieve higher operational intensity; however since the operator is already compute-bound, there is not much value in leveraging fusion (and the additional complexity). (3) We often need finer-granularity dataflow schemes to fit fused operator tensors on-chip; however fusing two activation-weight computation ($f(FC, FC)$) can trade-off (weight) reuse opportunity and may reduce actual achievable performance (§5.3.1).

Why not fuse multiple operators? We did not fuse multiple operators such as $f(L, A, O)$ or $f(K, L, A)$ for two

reasons. (1) Fusing L/A with FC such as $f(A, O)$ or $f(K, L)$ can drop the potential performance of FCs compared to their single operator performance (Figure 5). (2) The more operators we fuse, the more data we need to stage partially on-chip. Since the on-chip memory is often extremely limited, we need to execute the fused operators at a much finer granularity, which may lead to a degradation in achievable performance (§5.3.2). With these analyses, we decide to fuse only L and A.

4.2. Challenges with Tensor Fusion Implementation

Fusing L and A operators introduces two key challenges that we discuss here. §5 presents implementation details.

Challenge 1: Respecting data dependencies across operators. Fusing L and A causes its unique challenge of data dependency owing to the many-to-many Softmax operation between them (§3.2). Softmax requires a reduction along a specific dimension of the tensor before scaling individual elements. Arbitrary inter-loop tiling as employed by prior CONV/FC fusion techniques [8, 91] violates this data dependency constraint.

Challenge 2: Effectively handling large intermediate tensors that do not fit in on-chip memory. Recall that the intermediate tensor between L and A has size $O(BHN^2)$. As discussed in §3.3, this can easily exceed the on-chip memory capacity of DNN accelerators. Further, the specific size of the on-chip memory may be highly variable across different accelerators.

Owing to the above challenges, conventionally, we often do not apply tensor fusion to attention layer and stick to operator-by-operator operation scheme, as shown in Figure 6(a). In this work, we use FLAT to enable L-A fusion operation scheme, as in Figure 6(b). We describe details next.

5. FLAT Dataflow Implementation

To fuse two tensor operators X and Y , we divide the loop nests into two groups: outer-loop and inner-loop. We use L and A for illustration as shown in Figure 7, but the principles are applicable to any set of consecutive tensor operators. The outer-loops are shared across L and A. The inner-loops are unique for each operator. After fusion, the fused operator has two inner-loops, which we run one after another (interleaved), and iterate through the shared outer-loop. Considerations for tile sizes to address the data dependence and on-chip memory constraints (§4.2) are discussed in this section.

5.1. FLAT-tile and Execution Granularity

FLAT employs two levels of tiling: intra-operator tiling and inter-operator tiling. We name each tile in inter-operator tiling, a FLAT-tile. FLAT computes FLAT-tile activations from L and feeds it through Softmax and to A. FLAT-tiles, the inner-loop in Figure 7, essentially specifies how many

slices of the partial intermediate tensor are calculated in one pass of the fused-operator in Figure 6(b).

The minimum granularity of the FLAT-tile is determined by the data dependence constraint of Softmax and called *row-granularity* (discussed in §5.2), for effectively collecting a group/tile of (input) data that fulfills the Many-to-Many dependency pattern of Softmax. We progressively build larger (coarser-grain) tiles, namely, tiling multiple number of rows at a time (R_x), multiple number of heads (H_x), and finally, multiple number of (micro-)batches (B_x) in the tile. We refer to these as Row (R-Gran), Head (H-Gran), and Batch (B-Gran) granularity respectively (discussed in §5.3). Further, the most intuitive baseline of moving the entire intermediate tensor (namely the entire output of L) on-chip is referred to as Batch-Multi-Head granularity (M-Gran), as shown in Figure 7.

5.2. Managing Constraints from Data Dependency

Basic execution unit: Row-granularity. The Softmax reduction is along the key dimension: this effectively captures the relative weight of each token in the query sequence against other tokens in the key sequence. The minimum Softmax execution requires an $[1, N]$ input array, which in turn requires a query of $[1, D]$ and a key of $[D, N]$, as illustrated in Figure 1 Step-2 and Step-3². This forms our basic tiling unit (finest granularity)—*row-granularity*, which respects the data dependency introduced by the Softmax while keeping minimum number of elements to pass between L and A. FLAT restricts the tile sizes to operate in multiples of this row-granularity.

5.3. Managing Constraints from On-Chip Memory

5.3.1. M-Gran, B-Gran, H-Gran: Leveraging Limited Reuse of $f(L, A)$ Coarser granularities require staging larger tiles in the on-chip memory. As sequence lengths increase this can increase rapidly (recall the $O(N^2)$ growth). To fit into the limited on-chip memory, one may target finer granularities, e.g., moving from M-Gran to B-Gran (i.e., effectively tiling micro-batches). In general, while this helps reduce the size of the tile, when we are tiling two operators at finer granularity at the outer-loop, we may trade-off the reuse opportunity at the inner-loops. For example, for $f(FC, FC)$ and $f(CONV, CONV)$, when decreasing the batch size (i.e., micro-batching), we directly reduce the number of times a weight can be reused. The weights need to be re-fetched again and again for each micro-batch. This effect is exacerbated when considering finer granularities such as H-Gran for the weight-activation $K/Q/V/O$ operators. The reduced reuse opportunity by inter-operator tiling reduces the achievable performance, even though the fused operator has large operational intensity (Figure 5). In contrast, L and A are

²Note that here we are describing fused L-A operators, where the K, Q, and V tensors are already calculated and prepared in Step-1.

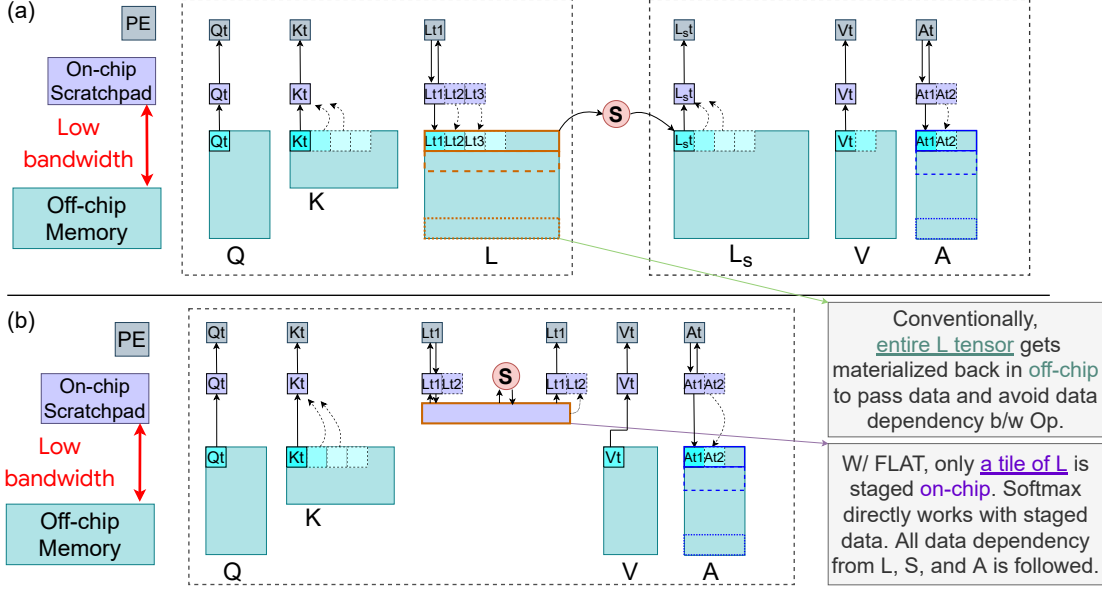


Fig. 6: (a) Baseline and (b) FLAT dataflow. FLAT performs inter-operator fusion of L , A while respecting data dependencies introduced by Softmax. FLAT-tile enables staging slices of the logits tensor in the on-chip scratchpad increasing effective memory bandwidth. This fused, interleaved execution of L , A yields higher compute utilization and improved performance.

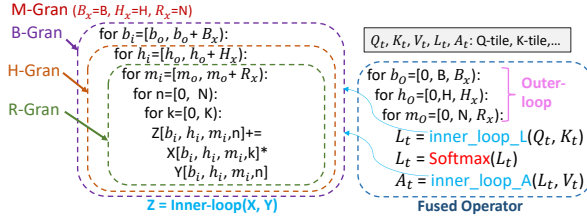


Fig. 7: For loop of fused L-Softmax-A (or shortened as L-A in the paper) and the choice of granularity.

activation-activation operations (§3.1.2). Each new activation of L needs to compute with a new activation of A , i.e., there are no reuse opportunities at the algorithmic level. Decreasing the tiling granularity (M-Gran to B-Gran to H-Gran), does not preclude any reuse opportunity, since there are no reuse opportunities at the algorithmic level. Thus, the finer M-Gran, B-Gran, H-Gran in FLAT are well-suited for $f(L, A)$.

5.3.2. R-Gran: Extreme Large Sequence Range To enable very long sequence lengths [20, 48, 64], but with limited on-chip memory resources [42, 80], we need to tile at even finer granularity, namely R-Gran. However, finer granularities come with an associated trade-off: when we reduce the number of rows (R_x), we will also reduce the reuse opportunity in the matrix multiplication itself. For example, even for L/A fusion, using fewer rows means the same key vectors need to be fetched multiple times across the interleaved cross-operator outer loops. Further, reducing number of rows at the outer-loop could also decrease the achievable performance at the inner-

Table 1: Buffer requirement for tiling granularity. M: batched Multi-head, B: Batch, H: Head, R: Row.

Granularity	M-Gran	B-Gran	H-Gran	R-Gran
Buffer Requirement	$O(8BDN+BHN^2)$	$O(8DN+HN^2)$	$O(8Nd+N^2)$	$O(4Rd+4Nd+RN)$

loop, e.g., not enough dimension size to fully utilize PE array. Thus, FLAT co-explores inter-operator (optimizing the outer-loop) and intra-operator dataflow (optimizing the inner-loop) to mitigate these potential sources of inefficiencies.

5.3.3. On-chip Buffer Requirement Table 1 lists the required on-chip buffer size using FLAT. We derive the R-Gran value here (others follow similar reasoning). L operator consumes $(Rd+Nd) \times 2$ size of the on-chip buffer (2 to account for double buffering), and A consumes $(Nd+Rd) \times 2$. RN for buffering the intermediate tensor (FLAT-tile) (no double buffering since it does not interact with off-chip memory), whose on-chip buffer requirement is shown in Table 1.

5.4. HW support to implement FLAT

FLAT requires minimal HW support: (1) controller to recognize our fine-grained dataflow, and (2) on-chip buffer to be *software-addressable* to support tiling. These features are already supported by most accelerators [9, 42, 71, 80].

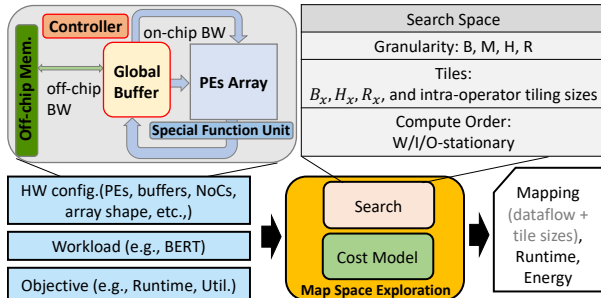


Fig. 8: Map space exploration framework. (Special Function Unit: for computing non-linear operations, e.g., softmax, activations.)

6. Evaluation Methodology

6.1. Modeling Methodology

Accelerator simulation. We developed a detailed analytical cost model to estimate the performance and energy consumption of FLAT across a range of hardware accelerators configurations, following the same methodology as prior work [3, 59]. We meticulously model the major microarchitectural blocks commonly shared by most DNN accelerators as outlined in Figure 8. Based on this model, we collect the relevant architectural details, which later are used to compute the accelerator performance metrics. Using this simulation methodology enables us to study and grasp the key differences across a range of dataflow optimizations, while supporting different classes of hardware accelerators, including TPU-v3 [42], Eyeriss [17], Simba [71]. One of the key features of our simulation methodology is the detailed modeling of the accelerator memory hierarchy to systematically assess the memory-boundedness of attention operators and their pressure on off-chip memory bandwidth.

Energy model. Collecting the detailed activity counts from the analytical model, we use Accelergy [94] framework to estimate the energy consumption for the major microarchitectural blocks. That includes compute, on-chip memory, and off-chip memory communications. Note that FLAT neither alter the total number of computations nor the total number of accesses to the global buffer. Instead, it optimizes the number of off-chip memory accesses, which is the major contributor to the overall accelerator energy consumption [15, 77].

Comparison to prior work. There are several popular open-sourced DNN accelerator modeling frameworks, such as Timeloop [59], MAESTRO [3], and others [23, 57, 69, 95]. However, they have limited support for cross-operator fusion or cross-layer performance modeling. For example, Timeloop [59] and MAESTRO [3] only model the performance of an accelerator in a single-layer manner, which narrows their application in modeling fusion opportunities. In contrast, our framework evaluates

the performance of DNN models in both single-layer and cross-layer manner, enabling various cross-operator fusion studies. To ensure the integrity and correctness of our framework, we compared the simulation results from our framework under single-layer modeling to MAESTRO [3]. The performance metrics are within 1% difference to MAESTRO’s results.

Workloads. We study a range of recent attention-based models, including BERT-Base [81] (BERT), TransformerXL [22] (TrXL), FlauBERT [54], T5 [65] (T5), and XLM-MLM-En [53] (XLM). We evaluate these models under different sequences lengths ranging from $N = 512$ to $N = 64K$ to imitate attention-based models with long sequence length [11, 48]. We also study a future-proofing sequence length of size $N = 256K$. We use a batch size of 64 for all the models. Note that the batch size choice is immaterial to our dataflow optimization.

Accelerator configurations. We evaluate the benefits of FLAT on two different accelerator regimes, namely cloud and edge accelerators. As outlined in Table 2, we set the accelerator configurations in our model following the designs proposed for cloud [42, 80] and edge [2, 16, 96] accelerators. In all the evaluations, we allot sufficient FLOPs to the Special Function Unit (Figure 8) in order to eradicate the expected compute bottlenecks, uniformly across all the dataflow variants.

Evaluation metrics. For all the evaluations, we use performance and energy savings as efficiency metrics. For comparisons between different models, we normalize the runtime of each dataflow by the ideal runtime of the target workload as follows:

$$Util = \frac{Runtime_{ideal}}{Runtime_{dataflow}}$$

; where $Runtime_{ideal}$ is the arithmetic optimal runtime of the current workload. That is, the total computes in a model divided by the peak FLOPs of the target accelerator. $Runtime_{dataflow}$ represents the achieved runtime by a dataflow optimization. This *normalized runtime* metric explains how far the current dataflow is from its arithmetic optimum. This metric is an indication of the distance to the dataflow compute-boundary in the roofline model as well as compute resource utilization ($Util$).

Map-space exploration workflow. We also integrate a map-space exploration (MSE) workflow (Figure 8) into our simulation framework. The main purpose of this exploration workflow is to carry out a search algorithm in a predefined map space governed by the cost model. In this work, we use exhaustive search to find the optimal design point uniformly across all the dataflow optimizations. MSE includes both intra- and inter-operator dataflow optimization space (enabling optimal dataflow comparisons with and without FLAT technique later in Table 3 and §7). The relevant architectural parameters for this optimization

space are outlined in [Figure 8](#).

6.2. Details of Major Microarchitectural Units

Compute model. We model the compute array as a collection of processing elements with configurable bandwidth from/to the global on-chip buffers. The compute array model supports common intra-operator dataflow, including weight, input, and output stationary. In addition, we model various data distribution and reduction NoCs, including systolic, tree, or crossbar structures to study the trade-offs between compute bandwidth and distribution-collection time [51, 52]. Following this methodology, we model TPU [43] (systolic-array) as well as other spatial array accelerators, such as Eyeriss v2 [16] and MAERI [52]). We also carefully model the overhead of switching tiles for filling and draining data to reflect the cold start and tailing effect. Finally, we account for softmax operation runtime in all the evaluations.

Buffering model. Studying dataflow optimization techniques demand for a detailed modeling of buffers. To achieve this objective, we model PE arrays with local scratchpad for input, weight, intermediate results, and output storage. We add the on-chip global buffer to store the intra- and inter-operator tiles. The performance model also includes the data spilling overhead. That is when the live memory footprint (buffer requirement for staging data on-chip) is larger than the on-chip global buffer capacity.

Memory bandwidth. Since there are multiple microarchitectural units that access the on-chip and off-chip memories, we model them as limited bandwidth shared-hardware resources. That is, if the access rate to a shared memory resource exceeds a pre-defined bandwidth, the data accesses are throttled. This overhead manifests as longer runtime.

6.3. Overview of the Evaluations

We organize the evaluation results as follows:

(1) **Efficacy of the FLAT dataflow (§7.1, §7.2, §7.3):** We first fix the “headline” “HW resources” (i.e., FLOPs and off-chip memory bandwidth) as outlined in [Table 2](#) and sweep-and-explore other microarchitectural parameters relevant to the dataflow efficiency, including on-chip memory size and dataflow variations (Naive, Flex, FLAT). The on-chip memory size assesses the dataflow optimizations associated to the large intermediate tensor size in the attention layers. We demonstrate the benefits of FLAT across a range of hardware and dataflow configurations, without biasing to any specific design point.

(2) **Concrete comparison of accelerator design points (§8):** Next, we pick two specific hardware design points, namely a cloud and an edge accelerator, with headline HW resources that closely resemble a TPU-v3 [42] and edge-TPU [2], respectively. For baseline design, we use the best possible dataflow optimization in the intra-operator map

Table 2: The HW resource configuration of cloud and edge accelerators in the evaluation sections.

Platform	Number of PEs	On-chip BW	Off-chip BW
Edge	32x32	1TB/sec	50GB/sec
Cloud	256x256	8TB/sec	400GB/sec

Table 3: Comparisons Dataflow Configurations.

Dataflow	Design Point	Description
Naïve (intra-operator dataflow)	Naive	Intra-operator weight-stationary dataflow with fixed tile size, seen in many DNN accelerators [1][2][27]
Flex (intra-operator dataflow)	Flex-opt	We exhaustively search for optimal intra-operator dataflow, reflecting the optimal solution can be found in existing intra-operator MSEs/mappers [31][37][45]
FLAT (intra- and inter-operator dataflow)	FLAT-opt	We exhaustively search for optimal intra-operator as well as inter-operator dataflow, enabled by FLAT.

space following prior techniques [1, 17, 25, 35, 38, 42, 44, 51, 59]. We call this performant baseline accelerator Flex-opt, against which we compare FLAT-opt, our proposed inter-operator and tiling dataflow optimization.

7. Evaluation I: FLAT Dataflow Efficacy

7.1. Utilization

Edge accelerator. As described in [§6.1](#), lower *Util* implies higher run time and lower throughput. [Figure 9](#) shows the utilization of different dataflow configurations (as outlined in [Table 3](#)). The Naive dataflow barely achieves to 0.2 utilization for a buffer size ≤ 10 MB. Increasing the on-chip buffer to an excessive 100 MB yields a peak utilization of merely 0.6 for this dataflow. This low utilization is mainly attributed to the bandwidth-boundedness of attention operations when no dataflow optimization is employed.

Leveraging efficient staging of tensor in on-chip memory, Flex-M can potentially increase the utilization. However, when the on-chip buffer size is not sufficiently sized

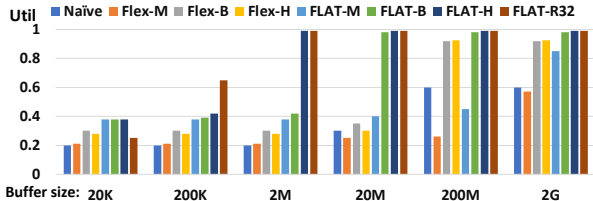


Fig. 9: Compute utilization analysis of L-A operators under different dataflow granularities, running BERT with 512 sequence length with edge platform resources. Flex dataflow (Flex-X): Flex dataflow with X-granularity. FLAT dataflow (FLAT-X): Flex dataflow with X-granularity; X could be M (batch-Multi-head), B (Batch), H (head), or R (row).

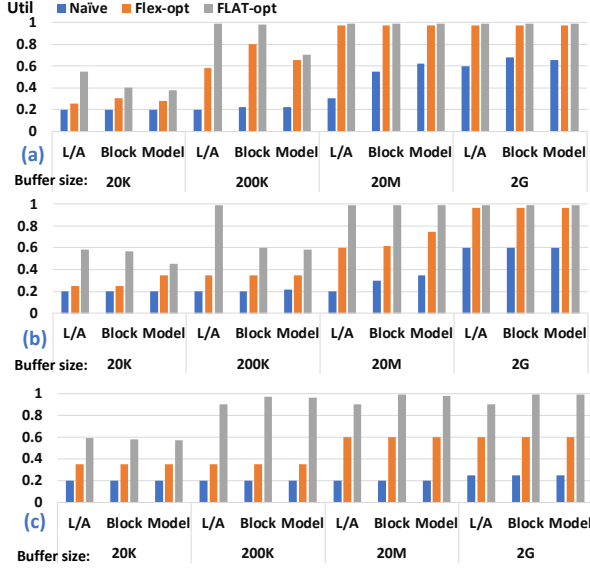


Fig. 10: Comparisons of compute utilization across different sequence lengths running BERT under edge platform resources with sequence length of (a) 512, (b) 4K, and (c) 64K. We sweep the available on-chip buffer from size 20KB to 2GB. We list three level of performance analysis, L-A: focusing on performance difference at the L, A operators; Block: consider all operators in the attention block; and Model: a model-wise performance.

to house the intermediate tensors, the accelerator requires to fetch the intermediate tensors partially from the on-chip memory and the rest from off-chip memory breaking into the limited off-chip bandwidth wall. Compared to Naive dataflow, this extra pass between on-chip and off-chip memories diminishes the potential benefits of Flex-M under tightly-budgeted on-chip buffers scenarios. As we can see in Figure 9, even increasing the on-chip buffer capacity to 2 GB is not adequate to fulfill the on-chip buffer size requirement for Flex-M. Flex-B and Flex-H are two variants with finer granularity of storing the intermediate results. They have smaller memory footprint for on-chip buffer that translates to a reduction in the buffer requirement to around 160 MB, while reaching to 0.92 utilization, comparing to 0.6 utilization with 100 MB on-chip storage with Naive dataflow.

Comparing to Flex which only exploits single operation execution (intra-operator), FLAT further enables cross-operator execution (inter-operator), which gains cross-operator data reuse opportunity and reduces the off-chip memory access. The fine-grained execution schemes of FLAT significantly reduces the on-chip buffer requirement, from 2 GB (Naive) and 160 MB (Flex-H) to just 0.6 MB (FLAT-Rx). These results show the effectiveness of cross-operator data reuse in mitigating the bandwidth-boundedness and improving the utilization from 0.6 (Naive) and 0.92 (Flex-H) to a nearly optimal

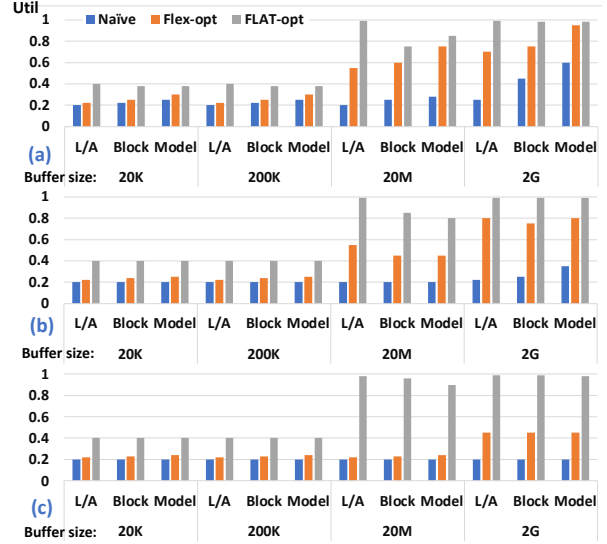


Fig. 11: Comparisons of compute utilization across different sequence lengths running XLM under cloud platform resources with sequence length of (a) 4K, (b) 16K, (c) 256K.

value of 0.99 (FLAT-Rx).

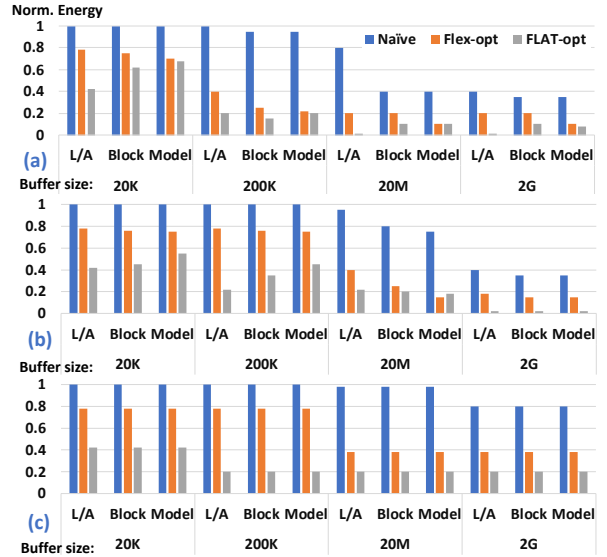


Fig. 12: The corresponding energy consumption of each of the data-point in Figure 10. The energy numbers are normalized by the largest energy number in each sub-plot.

Sensitivity to sequence length. Note that, Flex-opt and FLAT-opt represents the optimal design points in the Flex and FLAT dataflow design space, respectively. Figure 10 and Figure 11 compare the compute utilization of these dataflows by sweeping the sequence length for an edge and cloud accelerators, respectively. Flex design space exhaustively has both dataflows of state-of-the-art DNN

accelerators [1, 17, 25, 35, 38, 42, 44, 51, 59] as well as their other relevant configurations. On the other hand, Flex-opt represents the most optimal design point across all the evaluations.

As Figure 10 shows, FLAT-opt consistently outperforms Naive and Flex-opt. Analyzing the results indicate that though tensor-tensor fusion seems to be complicated and deemed as non-profitable, FLAT can efficiently execute tensor-tensor fusion in attention layers and harvest the highest performance gains. In Figure 10, as the sequence length increases, the on-chip buffer requirement increases quickly (Table 1). Under this scenario, most of the accelerator design points in Flex design space starts to hit the memory boundedness. However, applying the FLAT technique, we can effectively reduce the memory requirement and thus providing a better scalability to sequence length. At the optimal design point (FLAT-opt) reaches nearly 1.0 compute utilization with $10\times-100\times$ less on-chip buffer requirement, a scarce and critical hardware resource for accelerators, compared to Flex-opt.

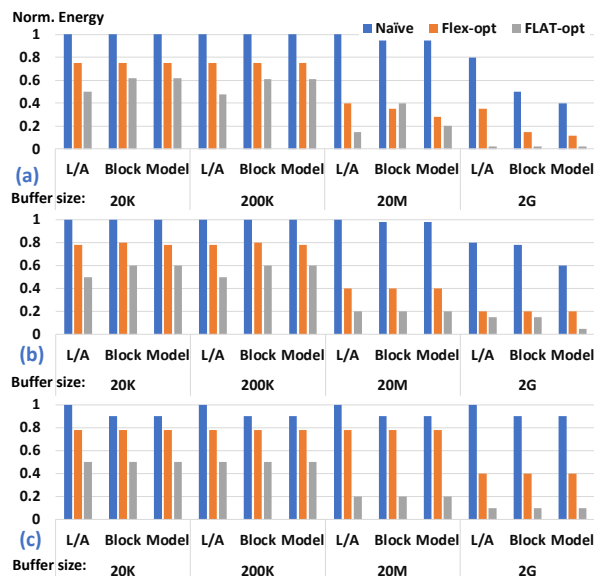


Fig. 13: The corresponding energy consumption of each of the data-point in Figure 11. The energy numbers are normalized by the largest energy number in each subplot.

Sensitivity to different operator fusion. So far, we analyze the operator fusion for only L and A operators, while keeping all the other attention operators non-fused (See the justification for this decision in §4.1). As shown in the first row of Figure 10 from left to right, we observe that the effect of L/A operators are diluted as more operator fusions are unlocked. In attention-based models, FC/GEMM and attention operators, namely L and A, are generally the most dominant computation. For FC/GEMM, the typical single (intra-)operator dataflow is often sufficient to

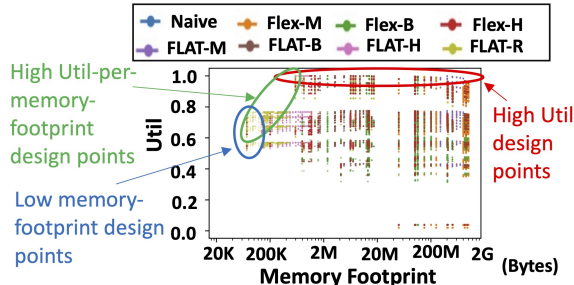


Fig. 14: The design space of FLAT when running BERT with sequence length of 512 under edge platform resources. Flex dataflow (Flex-X): Flex dataflow with X-granularity. FLAT dataflow (FLAT-X): Flex dataflow with X-granularity, where X could be M (batch-Multi-head), B (Batch), H (head), or R (row). The design-point with the highest utilization, given a buffer constraint represents Flex-Opt and FLAT-Opt (Table 3).

reach a high compute utilization, and hence FLAT-opt and Flex-opt performs equally well for these operators. As we can see, for the sequence length below 512, both Block-level and Model-level performance is dominated by FC/GEMM operators. Therefore, the gains from Flex-opt and FLAT-opt are immaterial. The significant gains from our approach emerge when the sequence length increases beyond 512 to 4K, 16K, and to 64K. Under these long-sequence lengths, the runtime contribution of L and A operators grows from 12% to 49%, 79%, and 94%, respectively. This increase causes our proposed FLAT-opt to outperform Flex-opt significantly even in Block and Model level scenarios.

Cloud accelerator. Figure 11 shows the evaluation of different dataflow optimizations for a cloud platform when the sequence length ranges from 4K to 256K. For L/A, Flex-opt reaches to nearly 0.8 utilization, however with the contingency of a 2GB on-chip buffer requirement. Moreover, when the sequence length surpasses 16K, the peak utilization reduces to around 0.6. On the other hand, FLAT-opt reaches to nearly 1.0 utilization, while significantly reduces the on-chip buffer requirement by $100\times-1000\times$ comparing to Flex-opt.

7.2. Energy Consumption

Figure 12 and Figure 13 show the corresponding energy consumption for the data points in Figure 10 and Figure 11, respectively. It is worth to mention that high utilization does not directly translate to better energy savings; however, highly correlated. Data points with high compute utilization generally employ better memory access patterns (e.g., less off-chip memory access and better data reuse) and thus impose less cost in terms of memory access energy, the dominant contributor to the overall energy consumption of DNN accelerators. In Figure 12 and Figure 13, we observe that FLAT-opt reduces the energy consumption by around $1.5\times-2.0\times$ comparing to

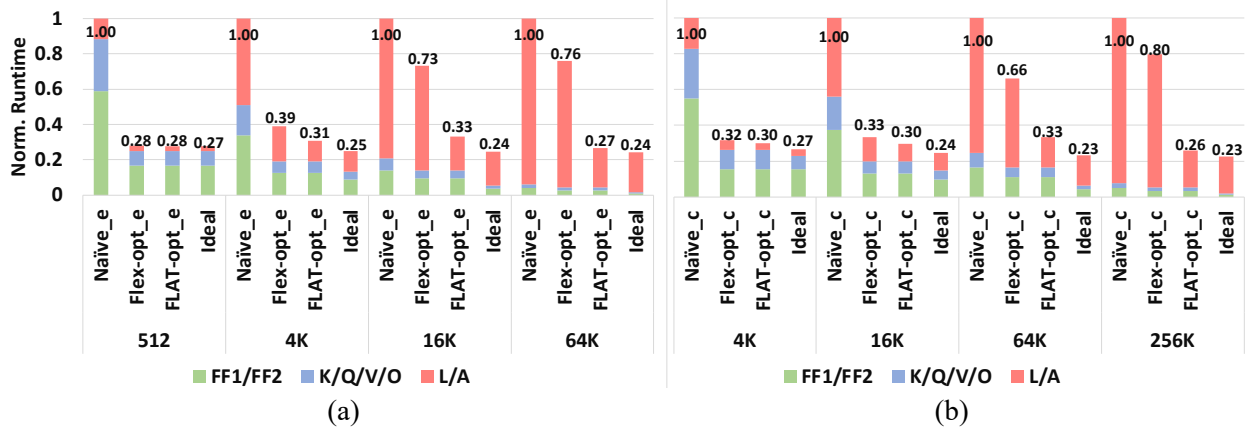


Fig. 15: End-to-end latency breakdown running: (a) BERT on Edge accelerator, (b) XLM on Cloud accelerator. Naive_e(dge): Edge with Naive dataflow. Flex-opt_e(dge): Edge with optimal Flex dataflow. FLAT-opt_e(dge): Edge with optimal FLAT dataflow. Similarly, for Naive_c(oud) and so on. Flex-opt represents the best possible (SOTA) intra-operator dataflow obtained through exhaustive search of the intra-operator map-space. FLAT performs inter-operator L-A fusion to relieve memory-bandwidth boundedness and achieves lower run time. While FLAT realizes benefits even at modest sequence lengths, the gains are pronounced at larger sequence lengths.

Edge	Speedup (Ave. 1.75)					Energy Consumption Ratio (Ave. 0.56)				
SeqLen	512	4K	16K	64K	256K	512	4K	16K	64K	256K
Bert	1.02	1.27	2.21	2.84	3.10	0.98	0.78	0.44	0.34	0.31
TrXL	1.02	1.23	2.06	2.75	3.07	0.98	0.81	0.48	0.35	0.31
FlauBert	1.01	1.11	1.62	2.26	2.67	1.00	0.90	0.61	0.43	0.36
T5	1.03	1.34	2.40	2.93	3.13	0.97	0.74	0.41	0.33	0.31
XLM	1.00	1.05	1.35	1.87	2.38	1.00	0.95	0.74	0.52	0.31
Average	1.02	1.20	1.89	2.50	2.85	0.99	0.83	0.52	0.39	0.32
Cloud	Speedup (Ave. 1.65)					Energy Consumption Ratio (Ave. 0.45)				
Bert	1.16	1.38	1.46	2.23	2.72	0.71	0.68	0.11	0.34	0.27
TrXL	1.13	1.34	1.45	2.20	2.71	0.73	0.27	0.13	0.35	0.27
FlauBert	1.07	1.21	1.42	2.21	2.93	0.87	0.80	0.72	0.49	0.37
T5	1.18	1.43	1.48	2.26	2.73	0.69	0.66	0.50	0.33	0.27
XLM	1.02	1.06	1.13	1.98	3.09	0.97	0.89	0.78	0.50	0.31
Average	1.11	1.28	1.38	2.17	2.83	0.79	0.61	0.33	0.40	0.30

Speedup and energy consumption ratio of: (left) FLAT-opt_e over Flex-opt_e, and (right) FLAT-opt_c over Flex-opt_c.

Fig. 16: The end-to-end speedup and energy-consumption ratio of FLAT-opt_e(dge) over Flex-opt_e(dge) and FLAT-opt_c(oud) over Flex-opt_c(oud) on different models.

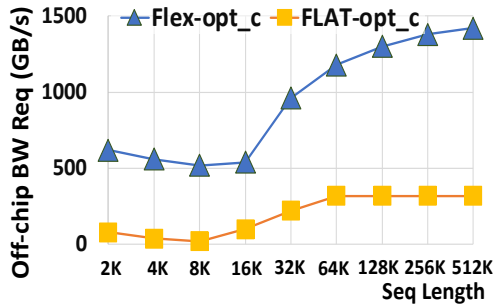


Fig. 17: The required BW to reach compute utilization rate higher than 0.95 in the most BW-intensive L-A operator when running XLM using Flex-opt_c(oud) or FLAT-opt_c(oud).

Flex-opt.

7.3. Map Space Exploration

Figure 14 shows a holistic view of the entire design space of FLAT dataflow. The top-left corner of the diagram indicates high utilization with the least memory footprint. For each dataflow, there are abundance of parameters that can be tuned under different optimization objectives and design constraints. For example, while in this work, we focus on maximizing the compute utilization, one may choose other objectives such as maximizing utilization normalized to memory footprint size, leading to points in the top-left corner, or the least memory footprint size, leading to points in the left-most region. From Figure 14, we can see that different dataflow configurations in the design space indeed represent notable differences in performance and memory requirement. This highlights the impact and importance of the design choices and dataflow optimizations.

8. Evaluation II: Accelerator Comparison

As shown in Table 2, we pick two common hardware configuration design points [2, 16, 42, 80, 96] and evaluate them for both edge and cloud accelerators. We fix the on-chip buffer capacity to 512KB [2] and 32MB [42] for edge and cloud accelerators, respectively. Analyzing these accelerators across different dataflow spaces, namely Naive, Flex, and FLAT, forms a concrete and reasonably realistic accelerator design space. Similar to previous sections, we call the optimal accelerator design point in each design space: Naive_edge, Flex-opt_edge, and FLAT-opt_edge for edge accelerator, and Naive_cloud, Flex-opt_cloud, and FLAT-opt_cloud for cloud accelerator, respectively.

Accelerator performance. As show in Figure 15(a), Flex-opt_edge and FLAT-opt_edge share the same normalized runtime for K/Q/V/O and FF1/FF2. This similarity in performance is because in FLAT-opt_edge, both K/Q/V/O and FF1/FF2 are treated as non-fused operators, and hence the map space for them are the same as the one in Flex-opt_edge. In edge accelerator, when the sequence length is 512, FLAT-opt_edge and Flex-opt_edge both reach a near optimal performance. However, when the sequence length increases to 4K, 16K, and 64K, the performance gap between FLAT-opt_edge and Flex-opt_edge widen. For example, at sequence length of 64K, FLAT-opt_edge runs $2.8\times$ faster than Flex-opt_edge, showing the efficiency of our dataflow optimization. In the cloud accelerator (Figure 15(b)), the performance difference between FLAT-opt_cloud and Flex-opt_cloud exaggerates even further. For example, at sequence length of 64K, FLAT-opt_cloud runs $3.07\times$ faster than Flex-opt_cloud. That is partly because of the larger model size for the cloud accelerator that enables FLAT-opt_cloud to better utilize the on-chip hardware resources.

Comparisons across different models. Figure 16 compares the performance of different dataflow optimizations across various transformer models. Compared to Flex-opt_edge, FLAT-opt_edge delivers $1.75\times$ speedup in edge accelerator, while significantly reducing the energy consumption by 44%. In cloud accelerator, FLAT-opt_cloud achieves $1.65\times$ speedup and 55% energy savings over Flex-opt_cloud. These results show the broad application of FLAT in improving the performance of various attention-based models under different design constraints.

Memory bandwidth requirement. Effectively using a limited off-chip bandwidth is an critical factor in the scalability of the hardware accelerator. That is because most DNN operations are often memory-bound and the off-chip memory bandwidth is often shared across different microarchitectural components in the system. In Figure 17, we show the peak off-chip bandwidth requirement to achieve a compute utilization over 0.95 for L and A attention operators. The left hand side of the U -shape of Fig-

ure 17 comes from the increase in the operational intensity and thus decrease of the bandwidth-boundedness as sequence length increases (§3.1). The right hand side of the U -shape of Figure 17 is caused by the quadratic and linear increase of on-chip memory requirement as sequence length increases for Flex and FLAT, respectively. On average, FLAT-opt_cloud reduces the off-chip bandwidth requirement by 82% against Flex-opt_cloud. Similarly, when evaluated under the edge scenario running BERT, FLAT-opt_edge achieves 71% reduction, on average, in the off-chip bandwidth requirement against Flex-opt_edge.

9. Related Works

Dataflow and mapping. Most work on DNN hardware dataflow techniques focus on individual CONV [1, 15, 23, 25, 28, 29, 40, 44, 56, 59, 71, 74, 83, 84, 95, 98] or GEMM [43, 90] operators. Some recent works consider fusion of multiple CONV operators and leveraged pipelined execution [8, 91]. Andrei et al. [39] studied operation fusion in Transformers—however, they only target operation fusion between MatMul operators and element-wise operators. Recently, Nvidia presented fused multi-head attention [4, 5]. Fusing multiple heads of the attention operators primarily involves adding an additional loop over the H independent heads, and considering the resultant operator as a single operator to explore intra-operator dataflow. This is captured by the Flex dataflow we evaluate. They, however, do not explore dependent MatMul-softmax-MatMul fusion, which is more complicated. FLAT targets such fusion and enables much higher performance.

Algorithmic optimization. Techniques such as quantization [47, 72, 97, 100], pruning [31, 68, 85, 86, 89], and distillation [41, 70, 76, 88] are used for compressing Attention-based models. There are a large body of algorithmic changes to attention mechanism [11, 18, 61, 63, 73], learned sparsity [21, 48, 67, 78] low-rank and kernel methods [19, 20, 45, 87], and others [11, 22, 64]. These techniques impact model quality and are orthogonal to the ideas developed in this paper. FLAT can be leveraged in association with these techniques when deployed on DNN accelerators to further improve run time and energy.

Attention accelerators. A^3 [32] and ELSA [33] propose dedicated attention accelerators and leverage approximate computation to accelerate attention layers, which trade-off run time performance with model quality. FLAT, by contrast, does not impact model quality, and is a generic yet powerful dataflow technique that can be leveraged on most existing accelerators.

Compiler optimizations. Fusion is a classic compiler technique widely employed in HPC [7, 24, 27, 46, 92] and ML compilers [6, 10, 14, 49]. However, in contrast to our work, ML compilers employ fusion in a limited fashion to fuse matrix operators (FC, CONV) with element-wise

operators [58].

10. Conclusion

We identify that running attention-based models with long sequences is challenging because of low reuse in certain attention operators and quadratic growth of intermediate memory footprint, both of which compound memory bandwidth requirements. We propose FLAT, a novel dataflow for attention layers employing inter-operator fusion (the first work to investigate this for attention layers), interleaved execution, and efficient tiling to enhance the operational intensity and provide high compute utilization, reduced off-chip bandwidth requirements and scalability to long sequence lengths.

References

- [1] Nvidia deep learning accelerator. <http://nvidia.org>, 2017.
- [2] Coral ai. <https://coral.ai/>, 2020.
- [3] Maestro: An open-source infrastructure for modeling dataflows within deep learning accelerators. <http://maestro.ece.gatech.edu/>, 2020.
- [4] Boosting nvidia mlperf training v1.1 performance with full stack optimization. <https://developer.nvidia.com/blog/boosting-mlperf-training-v1-1-performance-with-full-stack-optimization/>, 2021.
- [5] Nvidia fastertransformer. <https://github.com/NVIDIA/FasterTransformer>, 2021.
- [6] Tensorflow xla. <https://www.tensorflow.org/xla>, 2021.
- [7] Randy Allen and Ken Kennedy. Vector register allocation. *IEEE Computer Architecture Letters*, 41(10):1290–1317, 1992.
- [8] Manoj Alwani, Han Chen, Michael Ferdman, and Peter Milder. Fused-layer cnn accelerators. In *2016 49th Annual IEEE/ACM International Symposium on Microarchitecture (MICRO)*, pages 1–12. IEEE, 2016.
- [9] Eunjin Baek, Dongup Kwon, and Jangwoo Kim. A multi-neural network acceleration architecture. In *2020 ACM/IEEE 47th Annual International Symposium on Computer Architecture (ISCA)*, pages 940–953. IEEE, 2020.
- [10] Riyadh Baghdadi, Jessica Ray, Malek Ben Romdhane, Emanuele Del Sozzo, Abdurrahman Akkas, Yunming Zhang, Patricia Suriana, Shoab Kamil, and Saman Amarasinghe. Tiramisu: A polyhedral compiler for expressing fast and portable code. In *2019 IEEE/ACM International Symposium on Code Generation and Optimization (CGO)*, pages 193–205. IEEE, 2019.
- [11] Iz Beltagy, Matthew E Peters, and Arman Cohan. Longformer: The long-document transformer. *arXiv preprint arXiv:2004.05150*, 2020.
- [12] Prarthana Bhattacharyya, Chengjie Huang, and Krzysztof Czarnecki. Self-attention based context-aware 3d object detection. *arXiv preprint arXiv:2101.02672*, 2021.
- [13] Mark Chen, Alec Radford, Rewon Child, Jeffrey Wu, Heewoo Jun, David Luan, and Ilya Sutskever. Generative pretraining from pixels. In *International Conference on Machine Learning*, pages 1691–1703. PMLR, 2020.
- [14] Tianqi Chen, Lianmin Zheng, Eddie Yan, Ziheng Jiang, Thierry Moreau, Luis Ceze, Carlos Guestrin, and Arvind Krishnamurthy. Learning to optimize tensor programs. In *Advances in Neural Information Processing Systems*, pages 3389–3400, 2018.
- [15] Yu-Hsin Chen et al. Eyeriss: An energy-efficient reconfigurable accelerator for deep convolutional neural networks. *JSSC*, 52(1):127–138, 2016.
- [16] Yu-Hsin Chen, Tien-Ju Yang, Joel Emer, and Vivienne Sze. Eyeriss v2: A flexible accelerator for emerging deep neural networks on mobile devices. *IEEE Journal on Emerging and Selected Topics in Circuits and Systems*, 9(2):292–308, 2019.
- [17] Chen, Yu-Hsin and Krishna, Tushar and Emer, Joel and Sze, Vivienne. Eyeriss: An Energy-Efficient Reconfigurable Accelerator for Deep Convolutional Neural Networks. In *IEEE International Solid-State Circuits Conference, ISSCC 2016, Digest of Technical Papers*, pages 262–263, 2016.
- [18] Rewon Child, Scott Gray, Alec Radford, and Ilya Sutskever. Generating long sequences with sparse transformers. *arXiv preprint arXiv:1904.10509*, 2019.
- [19] Krzysztof Choromanski, Valerii Likhoshesterov, David Dohan, Xingyou Song, Jared Davis, Tamas Sarlos, David Belanger, Lucy Colwell, and Adrian Weller. Masked language modeling for proteins via linearly scalable long-context transformers. *arXiv preprint arXiv:2006.03555*, 2020.
- [20] Krzysztof Choromanski, Valerii Likhoshesterov, David Dohan, Xingyou Song, Andreea Gane, Tamas Sarlos, Peter Hawkins, Jared Davis, Afroz Mohiuddin, Lukasz Kaiser, et al. Rethinking attention with performers. *arXiv preprint arXiv:2009.14794*, 2020.
- [21] Gonçalo M Correia, Vlad Niculae, and André FT Martins. Adaptively sparse transformers. *arXiv preprint arXiv:1909.00015*, 2019.
- [22] Zihang Dai, Zhilin Yang, Yiming Yang, Jaime Carbonell, Quoc V Le, and Ruslan Salakhutdinov. Transformer-xl: Attentive language models beyond a fixed-length context. *arXiv preprint arXiv:1901.02860*, 2019.
- [23] Shail Dave, Youngbin Kim, Sasikanth Avancha, Kyoungwoo Lee, and Aviral Shrivastava. Dmazerunner: Executing perfectly nested loops on dataflow accelerators. *ACM Transactions on Embedded Computing Systems (TECS)*, 18(5s):1–27, 2019.
- [24] Chen Ding and Ken Kennedy. Improving effective bandwidth through compiler enhancement of global cache reuse. *Journal of Parallel and Distributed Computing*, 64(1):108–134, 2004.
- [25] Zidong Du, Robert Fasthuber, Tianshi Chen, Paolo Jenne, Ling Li, Tao Luo, Xiaobing Feng, Yunji Chen, and Olivier Temam. Shidiannao: Shifting vision processing closer to the sensor. In *International Symposium on Computer Architecture (ISCA)*, 2015.
- [26] Patrick Esser, Robin Rombach, and Björn Ommer. Taming transformers for high-resolution image synthesis. *arXiv preprint arXiv:2012.09841*, 2020.
- [27] Guang Gao, Russ Olsen, Vivek Sarkar, and Radhika Thekkath. Collective loop fusion for array contraction. In *International Workshop on Languages and Compilers for Parallel Computing*, pages 281–295. Springer, 1992.
- [28] Mingyu Gao et al. Tetris: Scalable and efficient neural network acceleration with 3d memory. In *ASPLOS*, pages 751–764, 2017.
- [29] Mingyu Gao et al. Tangram: Optimized coarse-grained dataflow for scalable nn accelerators. In *ASPLOS*, pages 807–820, 2019.
- [30] Ben Graham, Alaaeldin El-Nouby, Hugo Touvron, Pierre Stock, Armand Joulin, Hervé Jégou, and Matthijs Douze. Levit: a vision transformer in convnet’s clothing for faster inference. *arXiv preprint arXiv:2104.01136*, 2021.
- [31] Fu-Ming Guo, Sijia Liu, Finlay S Mungall, Xue Lin, and Yanzhi Wang. Reweighted proximal pruning for large-scale language representation. *arXiv preprint arXiv:1909.12486*, 2019.
- [32] Tae Jun Ham, Sung Jun Jung, Seonghak Kim, Young H Oh, Yeonhong Park, Yoonho Song, Jung-Hun Park, Sanghee Lee, Kyoung Park, Jae W Lee, et al. A³: Accelerating attention mechanisms in neural networks with approximation. In *2020 IEEE International Symposium on High Performance Computer Architecture (HPCA)*, pages 328–341. IEEE, 2020.
- [33] Tae Jun Ham, Yejin Lee, Seong Hoon Seo, Soosung Kim, Hyunji Choi, Sung Jun Jung, and Jae W Lee. Elsa: Hardware-software co-design for efficient, lightweight self-attention mechanism in neural networks. In *2021 ACM/IEEE 48th Annual International Symposium on Computer Architecture (ISCA)*, pages 692–705. IEEE, 2021.
- [34] Kaiming He, Xiangyu Zhang, Shaoqing Ren, and Jian Sun. Deep residual learning for image recognition. In *Proceedings of the IEEE conference on computer vision and pattern recognition*, pages 770–778, 2016.
- [35] Kartik Hegde, Po-An Tsai, Sitao Huang, Vikas Chandra, Angshuman Parashar, and Christopher W Fletcher. Mind mappings: Enabling efficient algorithm-accelerator mapping space search extended abstract.

- [36] Wen-Yi Hsiao, Jen-Yu Liu, Yin-Cheng Yeh, and Yi-Hsuan Yang. Compound word transformer: Learning to compose full-song music over dynamic directed hypergraphs. *arXiv preprint arXiv:2101.02402*, 2021.
- [37] Cheng-Zhi Anna Huang, Ashish Vaswani, Jakob Uszkoreit, Ian Simon, Curtis Hawthorne, Noam Shazeer, Andrew M Dai, Matthew D Hoffman, Monica Dinulescu, and Douglas Eck. Music transformer: Generating music with long-term structure. In *International Conference on Learning Representations*, 2018.
- [38] Qijing Huang, Minwoo Kang, Grace Dinh, Thomas Norell, Aravind Kalaiah, James Demmel, John Wawrzynek, and Yakun Sophia Shao. Cosa: Scheduling by constrained optimization for spatial accelerators. *arXiv preprint arXiv:2105.01898*, 2021.
- [39] Andrei Ivanov, Nikoli Dryden, Tal Ben-Nun, Shigang Li, and Torsten Hoefler. Data movement is all you need: A case study on optimizing transformers. *arXiv e-prints*, pages arXiv–2007, 2020.
- [40] Zhihao Jia, Matei Zaharia, and Alex Aiken. Beyond data and model parallelism for deep neural networks. *arXiv preprint arXiv:1807.05358*, 2018.
- [41] Xiaoyi Jiao, Yichun Yin, Lifeng Shang, Xin Jiang, Xiao Chen, Linlin Li, Fang Wang, and Qun Liu. Tinybert: Distilling bert for natural language understanding. *arXiv preprint arXiv:1909.10351*, 2019.
- [42] Norman P Jouppi, Doe Hyun Yoon, George Kurian, Sheng Li, Nishant Patil, James Laudon, Cliff Young, and David Patterson. A domain-specific supercomputer for training deep neural networks. *Communications of the ACM*, 63(7):67–78, 2020.
- [43] Norman P Jouppi, Cliff Young, Nishant Patil, David Patterson, Gaurav Agrawal, Raminder Bajwa, Sarah Bates, Suresh Bhatia, Nan Boden, Al Borchers, et al. In-datacenter performance analysis of a tensor processing unit. In *International Symposium on Computer Architecture (ISCA)*, pages 1–12. IEEE, 2017.
- [44] Sheng-Chun Kao and Tushar Krishna. Gamma: Automating the hw mapping of dnn models on accelerators via genetic algorithm. In *ICCAD*, 2020.
- [45] Angelos Katharopoulos, Aapo Vyas, Nikolaos Pappas, and François Fleuret. Transformers are rnns: Fast autoregressive transformers with linear attention. In *International Conference on Machine Learning*, pages 5156–5165. PMLR, 2020.
- [46] Ken Kennedy and Kathryn S McKinley. Maximizing loop parallelism and improving data locality via loop fusion and distribution. In *International Workshop on Languages and Compilers for Parallel Computing*, pages 301–320. Springer, 1993.
- [47] Sehoon Kim, Amir Gholami, Zhewei Yao, Michael W Mahoney, and Kurt Keutzer. I-bert: Integer-only bert quantization. *arXiv preprint arXiv:2101.01321*, 2021.
- [48] Nikita Kitaev, Łukasz Kaiser, and Anselm Levskaya. Reformer: The efficient transformer. *arXiv preprint arXiv:2001.04451*, 2020.
- [49] Fredrik Kjolstad, Shoaib Kamil, Stephen Chou, David Lugato, and Suman Amarasinghe. The tensor algebra compiler. *Proceedings of the ACM on Programming Languages*, 1(OOPSLA):1–29, 2017.
- [50] Tushar Krishna, Hyoukjun Kwon, Angshuman Parashar, Michael Pellauer, and Ananda Samajdar. *Data Orchestration in Deep Learning Accelerators*. Synthesis Lectures on Computer Architecture. Morgan & Claypool Publishers, 2020.
- [51] Hyoukjun Kwon, Prasanath Chatarasi, Michael Pellauer, Angshuman Parashar, Vivek Sarkar, and Tushar Krishna. Understanding reuse, performance, and hardware cost of dnn dataflow: A data-centric approach. In *Proceedings of the 52nd Annual IEEE/ACM International Symposium on Microarchitecture*, pages 754–768, 2019.
- [52] Hyoukjun Kwon, Ananda Samajdar, and Tushar Krishna. Maeri: Enabling flexible dataflow mapping over dnn accelerators via reconfigurable interconnects. *ACM SIGPLAN Notices*, 53(2):461–475, 2018.
- [53] Guillaume Lample and Alexis Conneau. Cross-lingual language model pretraining. *arXiv preprint arXiv:1901.07291*, 2019.
- [54] Hang Le, Loïc Vial, Jibril Frej, Vincent Segonne, Maximin Coavoux, Benjamin Lecouteux, Alexandre Allauzen, Benoît Crabbé, Laurent Besacier, and Didier Schwab. Flaubert: Unsupervised language model pre-training for french. *arXiv preprint arXiv:1912.05372*, 2019.
- [55] Peter J Liu, Mohammad Saleh, Etienne Pot, Ben Goodrich, Ryan Sepassi, Łukasz Kaiser, and Noam Shazeer. Generating wikipedia by summarizing long sequences. *arXiv preprint arXiv:1801.10198*, 2018.
- [56] Wenyang Lu et al. Flexflow: A flexible dataflow accelerator architecture for convolutional neural networks. In *HPCA*, pages 553–564. IEEE, 2017.
- [57] Linyan Mei, Pouya Houshmand, Vikram Jain, Sebastian Giraldo, and Marian Verhelst. Zigzag: A memory-centric rapid dnn accelerator design space exploration framework. *arXiv preprint arXiv:2007.11360*, 2020.
- [58] Wei Niu, Jiexiong Guan, Yanzhi Wang, Gagan Agrawal, and Bin Ren. Dnnfusion: accelerating deep neural networks execution with advanced operator fusion. In *Proceedings of the 42nd ACM SIGPLAN International Conference on Programming Language Design and Implementation*, pages 883–898, 2021.
- [59] Angshuman Parashar, Priyanka Raina, Yakun Sophia Shao, Yu-Hsin Chen, Victor A Ying, Anurag Mukkara, Rangharaj Venkatesan, Bruce Khailany, Stephen W Keckler, and Joel Emer. Timeloop: A systematic approach to dnn accelerator evaluation. In *2019 IEEE International Symposium on Performance Analysis of Systems and Software (ISPASS)*, pages 304–315. IEEE, 2019.
- [60] Niki Parmar, Ashish Vaswani, Jakob Uszkoreit, Łukasz Kaiser, Noam Shazeer, Alexander Ku, and Dustin Tran. Image transformer. *arXiv preprint arXiv:1802.05751*, 2018.
- [61] Niki Parmar, Ashish Vaswani, Jakob Uszkoreit, Łukasz Kaiser, Noam Shazeer, Alexander Ku, and Dustin Tran. Image transformer. In *International Conference on Machine Learning*, pages 4055–4064. PMLR, 2018.
- [62] Eric Qin, Ananda Samajdar, Hyoukjun Kwon, Vineet Nadella, Sudarshan Srinivasan, Dipankar Das, Bharat Kaul, and Tushar Krishna. Sigma: A sparse and irregular gemm accelerator with flexible interconnects for dnn training.
- [63] Jiezhong Qiu, Hao Ma, Omer Levy, Scott Wen-tau Yih, Sinong Wang, and Jie Tang. Blockwise self-attention for long document understanding. *arXiv preprint arXiv:1911.02972*, 2019.
- [64] Jack W Rae, Anna Potapenko, Siddhant M Jayakumar, and Timothy P Lillicrap. Compressive transformers for long-range sequence modelling. *arXiv preprint arXiv:1911.05507*, 2019.
- [65] Colin Raffel, Noam Shazeer, Adam Roberts, Katherine Lee, Sharan Narang, Michael Matena, Yanqi Zhou, Wei Li, and Peter J Liu. Exploring the limits of transfer learning with a unified text-to-text transformer. *arXiv preprint arXiv:1910.10683*, 2019.
- [66] Jonathan Ragan-Kelley, Connelly Barnes, Andrew Adams, Sylvain Paris, Frédéric Durand, and Suman Amarasinghe. Halide: a language and compiler for optimizing parallelism, locality, and recomputation in image processing pipelines. *Acm Sigplan Notices*, 48(6):519–530, 2013.
- [67] Aurko Roy, Mohammad Saffar, Ashish Vaswani, and David Grangier. Efficient content-based sparse attention with routing transformers. *Transactions of the Association for Computational Linguistics*, 9:53–68, 2021.
- [68] Hassan Sajjad, Fahim Dalvi, Nadir Durrani, and Preslav Nakov. Poor man’s bert: Smaller and faster transformer models. *arXiv preprint arXiv:2004.03844*, 2020.
- [69] Ananda Samajdar, Yuhao Zhu, Paul Whatmough, Matthew Matina, and Tushar Krishna. Scale-sim: Systolic cnn accelerator simulator. *arXiv preprint arXiv:1811.02883*, 2018.
- [70] Victor Sanh, Lysandre Debut, Julien Chaumond, and Thomas Wolf. Distilbert, a distilled version of bert: smaller, faster, cheaper and lighter. *arXiv preprint arXiv:1910.01108*, 2019.
- [71] Yakun Sophia Shao et al. Simba: Scaling deep-learning inference with multi-chip-module-based architecture. In *MICRO*, pages 14–27, 2019.
- [72] Sheng Shen, Zhen Dong, Jiayu Ye, Linjian Ma, Zhewei Yao, Amir Gholami, Michael W Mahoney, and Kurt Keutzer. Q-bert: Hessian based ultra low precision quantization of bert. In *Proceedings of the AAAI Conference on Artificial Intelligence*, volume 34, pages 8815–8821, 2020.
- [73] Tao Shen, Tianyi Zhou, Guodong Long, Jing Jiang, and Chengqi Zhang. Bi-directional block self-attention for fast and memory-efficient sequence modeling. *arXiv preprint arXiv:1804.00857*, 2018.

- [74] Linghao Song et al. HyPar: Towards hybrid parallelism for deep learning accelerator array. In *HPCA*, pages 56–68. IEEE, 2019.
- [75] Peize Sun, Yi Jiang, Rufeng Zhang, Enze Xie, Jinkun Cao, Xinting Hu, Tao Kong, Zehuan Yuan, Changhu Wang, and Ping Luo. Transtrack: Multiple-object tracking with transformer. *arXiv preprint arXiv:2012.15460*, 2020.
- [76] Zhiqing Sun, Hongkun Yu, Xiaodan Song, Renjie Liu, Yiming Yang, and Denny Zhou. Mobilebert: a compact task-agnostic bert for resource-limited devices. *arXiv preprint arXiv:2004.02984*, 2020.
- [77] Vivienne Sze, Yu-Hsin Chen, Tien-Ju Yang, and Joel S. Emer. *Efficient Processing of Deep Neural Networks*. Synthesis Lectures on Computer Architecture. Morgan & Claypool Publishers, 2020.
- [78] Yi Tay, Dara Bahri, Donald Metzler, Da-Cheng Juan, Zhe Zhao, and Che Zheng. Synthesizer: Rethinking self-attention in transformer models. *arXiv preprint arXiv:2005.00743*, 2020.
- [79] Yi Tay, Mostafa Dehghani, Samira Abnar, Yikang Shen, Dara Bahri, Philip Pham, Jinfeng Rao, Liu Yang, Sebastian Ruder, and Donald Metzler. Long range arena: A benchmark for efficient transformers. *arXiv preprint arXiv:2011.04006*, 2020.
- [80] Nvidia Tesla. V100 gpu architecture. *Online verfügbar unter <http://images.nvidia.com/content/volta-architecture/pdf/volta-architecture-whitepaper.pdf>, zuletzt geprüft am, 21, 2018*.
- [81] Ashish Vaswani, Noam Shazeer, Niki Parmar, Jakob Uszkoreit, Llion Jones, Aidan N Gomez, Łukasz Kaiser, and Illia Polosukhin. Attention is all you need. In *Advances in neural information processing systems*, pages 5998–6008, 2017.
- [82] Ashish Vaswani, Noam Shazeer, Niki Parmar, Jakob Uszkoreit, Llion Jones, Aidan N Gomez, Łukasz Kaiser, and Illia Polosukhin. Attention is all you need. In *Advances in neural information processing systems*, pages 5998–6008, 2017.
- [83] Swagath Venkataramani et al. Scaleddeep: A scalable compute architecture for learning and evaluating deep networks. In *MICRO*, pages 13–26, 2017.
- [84] Swagath Venkataramani et al. Deeptools: Compiler and execution runtime extensions for rapid ai accelerator. *IEEE Micro*, 39(5):102–111, 2019.
- [85] Hanrui Wang, Zhekai Zhang, and Song Han. Spatten: Efficient sparse attention architecture with cascade token and head pruning. *arXiv preprint arXiv:2012.09852*, 2020.
- [86] Hanrui Wang, Zhekai Zhang, and Song Han. Spatten: Efficient sparse attention architecture with cascade token and head pruning. In *2021 IEEE International Symposium on High-Performance Computer Architecture (HPCA)*, pages 97–110. IEEE, 2021.
- [87] Sinong Wang, Belinda Li, Madian Khabsa, Han Fang, and Hao Ma. Linformer: Self-attention with linear complexity. *arXiv preprint arXiv:2006.04768*, 2020.
- [88] Wenhui Wang, Furu Wei, Li Dong, Hangbo Bao, Nan Yang, and Ming Zhou. Minilm: Deep self-attention distillation for task-agnostic compression of pre-trained transformers. *arXiv preprint arXiv:2002.10957*, 2020.
- [89] Ziheng Wang, Jeremy Wohlwend, and Tao Lei. Structured pruning of large language models. *arXiv preprint arXiv:1910.04732*, 2019.
- [90] Xuechao Wei et al. Automated systolic array architecture synthesis for high throughput cnn inference on fpgas. In *DAC*, pages 1–6, 2017.
- [91] Xuechao Wei, Yun Liang, Xiuhong Li, Cody Hao Yu, Peng Zhang, and Jason Cong. Tgpa: tile-grained pipeline architecture for low latency cnn inference. In *Proceedings of the International Conference on Computer-Aided Design*, pages 1–8, 2018.
- [92] Michael Joseph Wolfe. *Optimizing supercompilers for supercomputers*. PhD thesis, University of Illinois at Urbana-Champaign, 1982.
- [93] Haiping Wu, Bin Xiao, Noel Codella, Mengchen Liu, Xiyang Dai, Lu Yuan, and Lei Zhang. Cvt: Introducing convolutions to vision transformers. *arXiv preprint arXiv:2103.15808*, 2021.
- [94] Yannan N. Wu, Joel S. Emer, and Vivienne Sze. Accelergy: An Architecture-Level Energy Estimation Methodology for Accelerator Designs. In *IEEE/ACM International Conference On Computer Aided Design (ICCAD)*, 2019.
- [95] Xuan Yang et al. Interstellar: Using halide’s scheduling language to analyze dnn accelerators. In *ASPLOS*, pages 369–383, 2020.
- [96] Amir Yazdanbakhsh, Kiran Seshadri, Berkin Akin, James Laudon, and Ravi Narayanaswami. An evaluation of edge tpu accelerators for convolutional neural networks. *arXiv preprint arXiv:2102.10423*, 2021.
- [97] Ofir Zafrir, Guy Boudoukh, Peter Izsak, and Moshe Wasserblat. Q8bert: Quantized 8bit bert. *arXiv preprint arXiv:1910.06188*, 2019.
- [98] Chen Zhang, Peng Li, Guangyu Sun, Yijin Guan, Bingjun Xiao, and Jason Cong. Optimizing fpga-based accelerator design for deep convolutional neural networks. In *Proceedings of the 2015 ACM/SIGDA International Symposium on Field-Programmable Gate Arrays*, pages 161–170, 2015.
- [99] Pengchuan Zhang, Xiyang Dai, Jianwei Yang, Bin Xiao, Lu Yuan, Lei Zhang, and Jianfeng Gao. Multi-scale vision longformer: A new vision transformer for high-resolution image encoding. *arXiv preprint arXiv:2103.15358*, 2021.
- [100] Wei Zhang, Lu Hou, Yichun Yin, Lifeng Shang, Xiao Chen, Xin Jiang, and Qun Liu. Ternarybert: Distillation-aware ultra-low bit bert. *arXiv preprint arXiv:2009.12812*, 2020.
- [101] Chen Zhu, Wei Ping, Chaowei Xiao, Mohammad Shoeybi, Tom Goldstein, Anima Anandkumar, and Bryan Catanzaro. Long-short transformer: Efficient transformers for language and vision. *Advances in Neural Information Processing Systems*, 34, 2021.
- [102] Xizhou Zhu, Weijie Su, Lewei Lu, Bin Li, Xiaogang Wang, and Jifeng Dai. Deformable detr: Deformable transformers for end-to-end object detection. *arXiv preprint arXiv:2010.04159*, 2020.